SDSS'Rio 2010 STABILITY AND DUCTILITY OF STEEL STRUCTURES
E. Batista, P. Vellasco, L. de Lima (Eds.)
Rio de Janeiro, Brazil, September 8 - 10, 2010

STABILITY OF STEEL COLUMNS SUBJECTED TO FIRE

Markus Knobloch*, Diego Somaini*, Jacqueline Pauli* and Mario Fontana*

* ETH Zürich, Institute of Structural Engineering – Steel, Timber and Composite Structures,
8093 Zurich, Switzerland
e-mails: knobloch@ibk.baug.ethz.ch, somaini@ibk.baug.ethz.ch,
pauli@ibk.baug.ethz.ch, fontana@ibk.baug.ethz.ch

Keywords: Fire, Structural design, Cross-sectional capacity, Flexural buckling.

Abstract. *The stability behavior of steel columns subjected to fire is strongly influenced by the distinct nonlinear stress-strain relationship of steel at elevated temperatures. The smaller proportional strain compared to ambient temperature and the very large strains required to reach so-called effective yield strength have a marked effect on the cross-sectional capacity and the overall flexural buckling behavior. The paper presents electrical furnace tests on stub columns in pure compression and slender columns in concentric and eccentric compression. The results show the influence of the nonlinear material behavior, the strain rate and thermal creep effects on the structural behavior of steel columns in fire.*

1 INTRODUCTION

Under fire conditions, unprotected steel members heat up quickly, primarily because of their high surface area-to-volume ratio and the good thermal conductivity of steel. At elevated temperatures, the strength and stiffness of steel decrease rapidly, and the almost linear elastic-perfectly plastic stress-strain relationship becomes distinctly nonlinear (e.g. [1]). As a result, the proportional limit is reached for smaller strains than at ambient temperature and large strains are required to reach so-called effective yield strength, both strongly influencing the stability behavior of steel columns in fire. Due to the smaller strains at proportional limit, the influence of plastification on the buckling behavior has to be considered up to larger buckling slenderness ratios than at ambient temperature. And even compact cross sections suitable for plastic design at ambient temperature develop local buckling at large strains required to reach so-called yield strength at elevated temperatures [2]. Therefore, the column strength in fire is limited due to both the critical buckling load considering overall flexural buckling in the plastic range and the cross-sectional capacity at elevated temperatures considering local buckling effects for compact sections.

The buckling behavior of concentrically and eccentrically loaded slender steel columns in fire is studied by Talamona et al. [3]. Based on their finite element results and a comparison to fire tests, Franssen et al. [4] develops a design model for steel columns whose stability failure mode is in the plane of the loading based on the Perry-Robertson principle, later adopted by EN 1993-1-2 [5]. Toh et al. [6] proposes a model for buckling strength in fire based on the Rankine approach. Simplified models usually base on ambient temperature design considering temperature-dependent reduction factors. Therefore, the models do not explicitly consider the nonlinear stress-strain relationship of steel at elevated temperatures and disregard local buckling effects of compact and semi-compact sections. These models are easy to use but have difficulty to precisely describe the structural behavior of steel columns subjected to fire.

A comprehensive analytical, experimental and numerical study analyzing the cross-sectional capacity of steel sections in axial compression and bending as well as the overall structural behavior of steel members at elevated temperatures in fire has been carried out at ETH Zürich. This paper analyses the critical buckling load of steel columns in fire and presents furnace test results on the cross-sectional capacity and slender column strength at elevated temperatures.

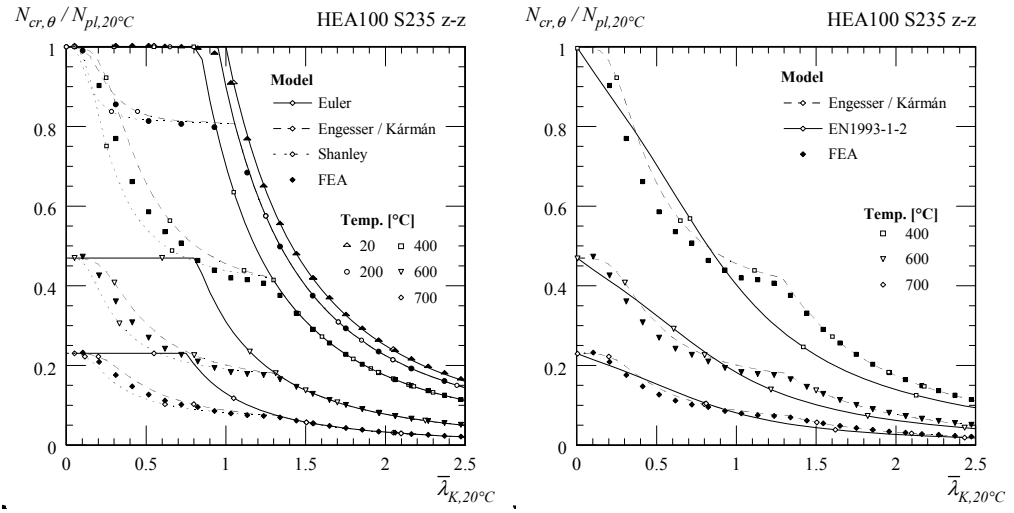

Figure 1: Critical buckling loads as a function of non-dimensional slenderness ratio at different temperatures according to Euler, Engesser/Kármán [8, 9], Shanley [7] and numerical simulations for a HEA 100 (S235) profile (left); Buckling strength calculated according to EN 1993-1-2 [5] at different temperatures compared to Engesser/Kármán and FEM results for a HEA 100 (S235) profile (right).

2 CRITICAL BUCKLING LOAD AT ELEVATED TEMPERATURE

The Euler formula for calculating the critical buckling load N_{cr} is fundamental for commonly used design models and is based on perfect linear elastic material behavior. Euler's formula leads to suitable results for the critical buckling load of slender steel columns at elevated temperatures (with uniform temperature distribution) which develop overall buckling at strains smaller than proportional strain ($\varepsilon_{Buckling} \leq \varepsilon_{p,fi}$). However, using Euler's formula for stocky and medium slender steel columns which develop buckling at larger strains ($\varepsilon_{Buckling} > \varepsilon_{p,fi}$) does not lead to suitable predictions of the critical buckling load due to the influence of the distinctly nonlinear stress-strain relationship of steel at elevated temperatures. Shanley [7], Engesser and Kármán [8,9] develop analytical models to determine the critical buckling load of cast iron columns that exhibit nonlinear material behavior as well. Their analytical models can easily be adapted for determining the critical buckling load of steel columns at elevated temperatures. Shanley's formula uses the tangent modulus and is a lower bound for the critical buckling load. Engesser's and Kármán's formula, however, substitutes the Young's modulus with their buckling modulus leading to an upper bound of the critical load. Figure 1 (left) shows the critical load $N_{cr,\theta}$ for buckling about the weak axis at elevated temperatures, given normalized to the plastic cross-sectional capacity at ambient temperature $N_{pl,20°C}$, for a HEA 100 steel column according to Euler's (continuous line), Shanley's (dotted line) and Engesser/Kármán's model (dashed line) considering temperature-dependent stress-strain relationships according to EN 1993-1-2 [5]. Additionally, the results of a numerical parametric study using the finite element approach (dots) are given. The numerical results are calculated with Abaqus, Rel. 6.8 using beam-elements (denoted as B31OS of the element library) and very small geometric imperfections (e_0 = L/50'000). The analytical and numerical results confirm that the critical buckling load of stocky and medium slender columns is strongly affected by the nonlinear material behaviour. Figure 1 (right) compares the Engesser's/Kármán's model and the FEM results to the buckling strengths according to EN 1993-1-2 [5] (continuous line). For medium slender columns the buckling strengths according to EN 1993-1-2 are larger than the critical buckling load at elevated temperatures.

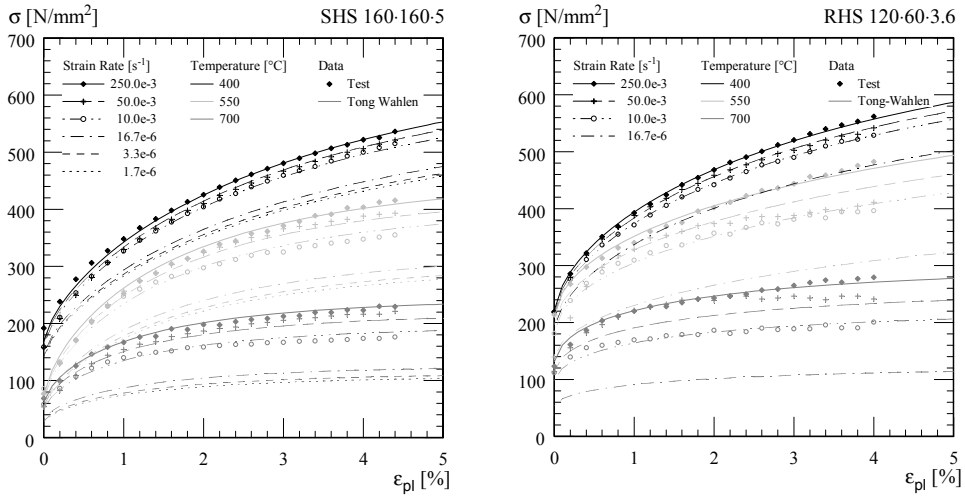

Figure 2: Stress-strain behaviour for 400, 550 and 700°C and different strain rates of the tested specimens cut from the SHS 160·160·5 (left) and RHS 120·60·3.6 (right) profile (dots) and calculated with the Tong-Wahlen model (lines).

3 EXPERIMENTAL INVESTIGATIONS

3.1 Material properties

Standard tensile material coupon tests at ambient and dilatometer compression tests at elevated temperatures were carried out at ETH Zürich to determine the basic engineering stress-strain behavior of the furnace test specimens. Material coupons were cut from the flat parts of the hot finished square and rectangular hollow sections (SHS 160·160·5 and RHS 120·60·3.6; steel grade S355) used for the structural furnace tests. Figure 2 shows the elevated temperature test results of the dilatometer tests performed on the SHS (left) and RHS (right) specimens. The nominal stress σ is given as a function of the plastic strain ε_{pl} for different temperatures and strain rates (dots). The nominal stress decreased with increasing temperature. For equal temperatures, the nominal stress decreased with decreasing strain rates indicating the strong influence of thermal creep effects on the stress-strain behavior. Only tests at high strain rates could be performed using the dilatometer. The Tong-Wahlen Model [10] was therefore used to determine the relationships between nominal stress and plastic strain at slower strain rates used for the structural furnace tests (see Figure 2, lines). Detailed test results are given in [11].

3.2 Stub column tests

A series of 11 stub column electric furnace tests on hot finished square (SHS 160·160·5) and rectangular (RHS 120·60·3.6) hollow sections (steel grade S355) at ambient and elevated temperatures under pure axial compression was performed at ETH Zürich. Wall thickness measurements were taken for each specimen. The average thicknesses were 5.3 mm for the SHS profiles and 3.8 mm for the RHS profiles leading to actual width-to-thickness ratios of 27 and 28. The length of the specimens was three times the nominal height of the cross section. End plates (270·270·20 mm) were welded to the ends of the specimens. Initial geometric imperfection measurements were taken using a three-dimensional video extensometer leading to maximal out-of-plane deflections between -0.3 and 0.3 mm.

The stub column electrical furnace tests were performed using a vertical reaction frame. Figure 3 shows the test setup which consists of the electric furnace with four heating zones (a), an hydraulic load jack (compression capacity 3 MN) at the bottom (b) and the reaction frame (c). Full axial load-end

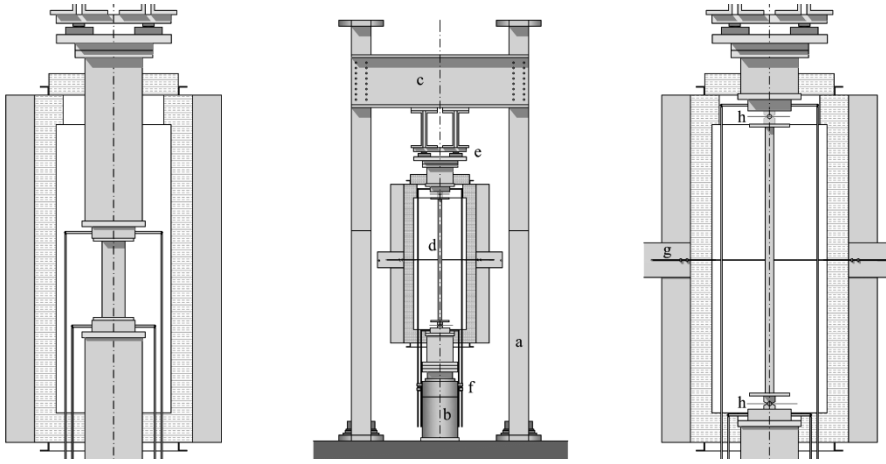

Figure 3: Setup of the stub and slender column tests; (a) electric furnace; (b) hydraulic load jack; (c) reaction frame; (d) test specimen; (e) load cells; (f) LVDT vertical; (g) LVDT horizontal; (h) roller bearing.

shortening histories were recorded, including the post-ultimate range. Two LVDTs (f) below the furnace determined the average end shortening of the stub columns recording the relative displacement at mid-heights of the parallel plates above and below the specimen. Four load cells (e) placed outside the furnace to protect them from heating measured the axial load. Three thermocouples glued on the specimen took the temperature measurement at the bottom, top and mid-height of one stub column surface.

Applying the steady-state method, the specimens were first uniformly heated to the temperatures of 400°C, 550°C and 700°C with a heating rate of 5°C/min (furnace air temperature). During the heating a very low constant axial pre-load of approximately 5kN was applied to the specimens. The thermal elongation during the heating was not restrained. After reaching the target temperatures, the axial load was applied to the stub columns with longitudinal strain rates of $16.7 \cdot 10^{-6}$, $3.3 \cdot 10^{-6}$ and $1.7 \cdot 10^{-6}$ s^{-1} (corresponding to 0.1 %/min, 0.02 %/min or 0.01 %/min) during the entire test. The different strain rates were used to analyze the influence of the thermal creep on the cross-sectional capacity at elevated temperatures.

Figure 4 shows the axial load-end shortening curves of the SHS (left) and RHS (right) test specimens. The main results of the stub column tests are summarized in Table 1. The ultimate loads at 400°C, 550°C and 700°C were reduced to 65%, 38% and 11% of the resistance at ambient temperature for the SHS profiles and to 84%, 53% and 15% for the RHS profiles. In addition, the axial load-end shortening behavior became more ductile and the load decreased less in the post-ultimate range with increasing

Table 1: Stub column test results - Measured area, ultimate load and strain at ultimate load.

Specimen	Temperature θ, [°C]	Strain rate $\dot{\varepsilon}$, [10^{-6} s^{-1}]	Area A, [mm^2]	Ultimate Load F_u, [kN]	Strain at F_u $\varepsilon_{tot,u}$, [%]	$F_u/N_{c,fi,2.0}$ [-]
SHS160_Stub_20C	20	16.7	3282	1225	0.36	1.01
SHS160_Stub_400C	400	16.7	3276	795	0.67	0.72
SHS160_Stub_550C	550	16.7	3276	468	0.64	0.61
SHS160_Stub_550Cs	550	3.3	3276	403	0.80	0.56
SHS160_Stub_550Css	550	1.7	3278	364	0.65	0.52
SHS160_Stub_700C	700	16.7	3288	138	0.72	0.46
SHS160_Stub_700Cs	700	3.3	3269	88	0.96	0.31
RHS120_Stub_20C	20	16.7	1311	483	0.48	0.96
RHS120_Stub_400C	400	16.7	1300	408	0.73	0.85
RHS120_Stub_550C	550	16.7	1303	257	0.81	0.79
RHS120_Stub_700C	700	16.7	1312	74	0.69	0.58

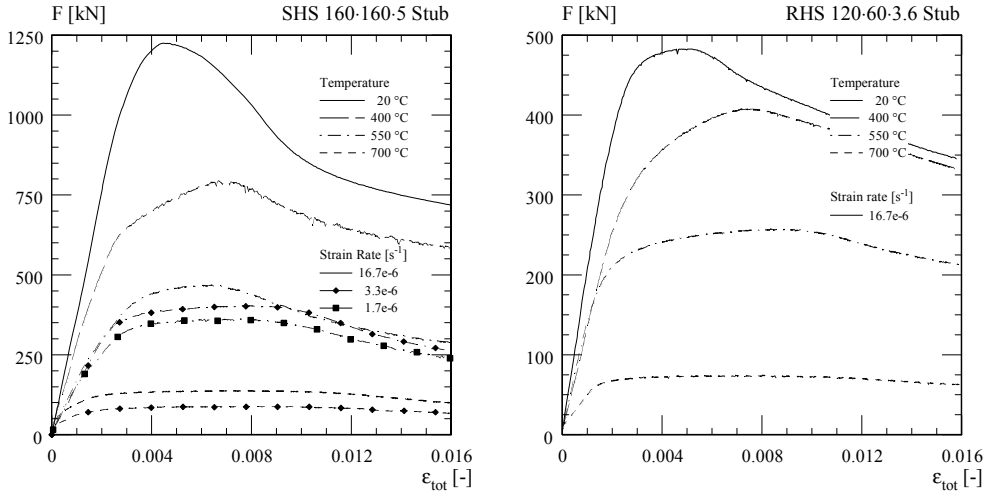

Figure 4: Axial load-end shortening curves of the SHS 160·160·5 (left) and the RHS 120·60·3.6 (right) stub column tests as a function of strain rate and temperature.

temperature. The strain rate markedly influenced the load-end shortening behavior and the ultimate load of the stub columns at 550° and 700°C. The ultimate loads determined with a strain rate of 0.02 %/min were approximately 14% (550°C) and 36% (700°C) lower than the resistance of the stub columns with a strain rate of 0.1 %/min. The ultimate load of the stub column at 550°C was additionally reduced by approximately 10% by reducing the strain rate from 0.02 %/min to 0.01 %/min. Table 1 additionally compares the ultimate loads F_u to the temperature-dependent cross-sectional resistance $N_{c,fi,2.0}$ calculated as the product of the actual area A and the actual stress reached at 2% strain $f_{2.0,\theta}$ considering the appropriate strain rate of each stub column test. The cross-sectional resistance $N_{c,fi,2.0}$ is not reached in the tests due to local buckling effects.

3.3 Slender column tests

A series of 16 slender column electric furnace tests (including 4 ambient temperature tests) under concentric and eccentric axial compression was performed at ETH Zürich on the same cross sections (from the same charges) used for the stub column tests. The lenght of the specimens was 1844 mm, the effective length of the test setup 1990 mm. End plates (270·270·20 mm) were welded to the ends of the specimens. The non-dimensional slenderness ratios about the weak axis at ambient temperature considering nominal values were 0.41 for the SHS and 1.05 for the RHS. Overall initial geometric imperfection measurements were taken along the central line of each face of the columns (see Table 2). The initial geometric imperfections were small and varied between approximately l/1´200 and l/10´000.

Steady-state slender column electrical furnace tests were performed using the same test setup and procedure used for the stub column tests, again leading to full axial load-end shortening histories. Horizontal displacement measurements were taken at mid-height on both sides of the column (see Figure 3g). Simply supported boundary conditions (about the weak axis of the cross sections) were realized using high-temperature resistant roller bearings (h). On the RHS profiles concentric and eccentric (10 and 50 mm) load tests were carried out. Tests using different strain rates (identical to the rates for the stub columns) to experimentally analyze the thermal creep effect were performed for the SHS profiles.

Figure 5 shows the axial load-end shortening curves of the SHS (left) and RHS (right) test specimens. The main results of the slender column tests are summarized in Table 2. The bending moment about the weak axis corresponding to the ultimate axial load F_u is calculated as the product of F_u and the

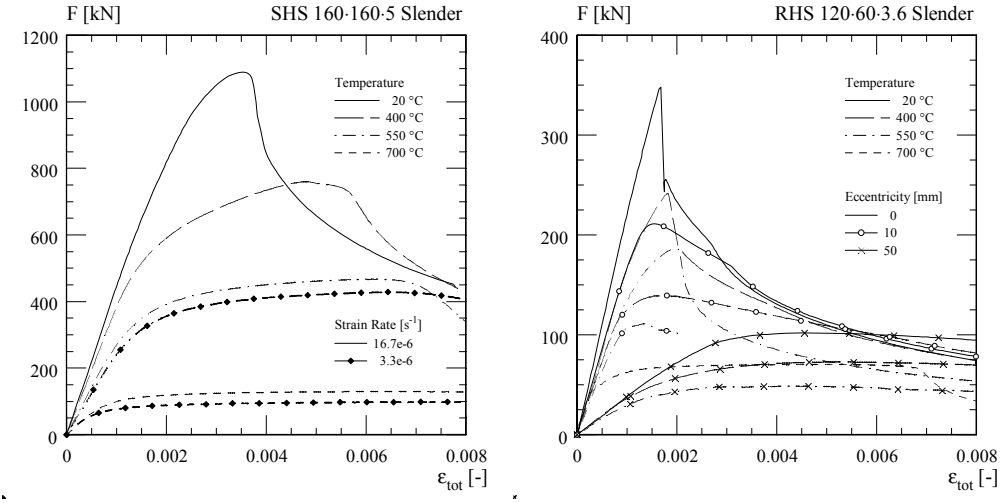

Figure 5: Axial load-end shortening curves of the SHS 160·160·5 slender column tests for different strain rates (left) and the RHS 120·60·3.6 slender column tests for different load eccentricities (right) as a function of temperature.

eccentricity e_1 ($M_{z,u,I}$) or the sum of the overall initial geometric imperfection about the weak axis $e_{0,z}$, eccentricity e_1 and deflection at ultimate load w_u ($M_{z,u,II}$). Due to the very small overall geometric imperfections (in addition to the relatively small overall slenderness), the SHS columns did not fail due to column buckling, but showed a failure mode governed by local buckling. The strain rate had again a marked effect on the ultimate load of the SHS profiles (see Figure 5 left). However, the thermal creep effect was less pronounced than for the stub column tests. The buckling strengths of the concentrically loaded RHS profiles at elevated temperatures were reduced to 70% (400°C), 53% (550°C) and 20% (700°C) of the strengths at ambient temperature.

Table 2: Slender column test results - Measured imperfections, ultimate load and strain and deflection at ultimate load, calculated bending moments at ultimate load

Specimen (SL: Slender)	Measured imperfection			Slender column tests				At ultimate load			
	strong axis	weak axis		Temperature	Eccentricity	Strain rate	Ultimate load	Strain	Deflection	Bending Moment	
	$e_{0,y}$ [mm]	$e_{0,z}$ [mm]	$l/e_{0,z}$ [-]	T [°C]	e_1 [mm]	$\dot{\varepsilon}$ [10^{-6} s^{-1}]	F_u [kN]	$\varepsilon_{tot,u}$ [%]	w_u [mm]	$M_{z,u,I}$ [kNm]	$M_{z,u,II}$ [kNm]
RHS160_SL_20C	0.30	0.61	3023	20	0	16.7	1089	0.35	0.4	0	1.1
RHS160_SL_400C	0.64	1.14	1618	400	0	16.7	760	0.48	6.0	0	5.4
RHS160_SL_550C	0.34	0.41	4498	550	0	16.7	467	0.62	1.2	0	0.7
RHS160_SL_550Cs	0.14	0.49	3763	550	0	3.3	428	0.64	4.8	0	2.3
RHS160_SL_700C	0.49	1.50	1229	700	0	16.7	130	0.61	6.5	0	0.9
RHS160_SL_700Cs	1.39	1.39	1327	700	0	3.3	98	0.70	0.7	0	0.2
RHS120_SL_20C	0.30	0.45	4098	20	0	16.7	348	0.17	4.0	0.0	1.5
RHS120_SL_20C_e10	1.29	0.36	5122	20	10	16.7	211	0.16	16.1	2.2	5.6
RHS120_SL_20C_e50	0.62	0.23	8017	20	50	16.7	102	0.47	32.6	5.1	8.4
RHS120_SL_400C	0.13	0.34	5424	400	0	16.7	242	0.18	5.0	0.0	1.3
RHS120_SL_400C_e10	0.35	0.41	4498	400	10	16.7	139	0.18	20.0	1.5	4.2
RHS120_SL_400C_e50	0.67	0.39	4728	400	50	16.7	73	0.51	35.1	3.7	6.2
RHS120_SL_550C	0.03	0.70	2634	550	0	16.7	186	0.20	5.7	0.0	1.2
RHS120_SL_550C_e10	0.66	0.19	9705	550	10	16.7	111	0.13	13.2	1.1	2.6
RHS120_SL_550C_e50	0.25	1.04	1773	550	50	16.7	49	0.43	29.0	2.5	3.9
RHS120_SL_700C	0.36	0.10	18440	700	0	16.7	71	0.41	1.4	0.0	0.1

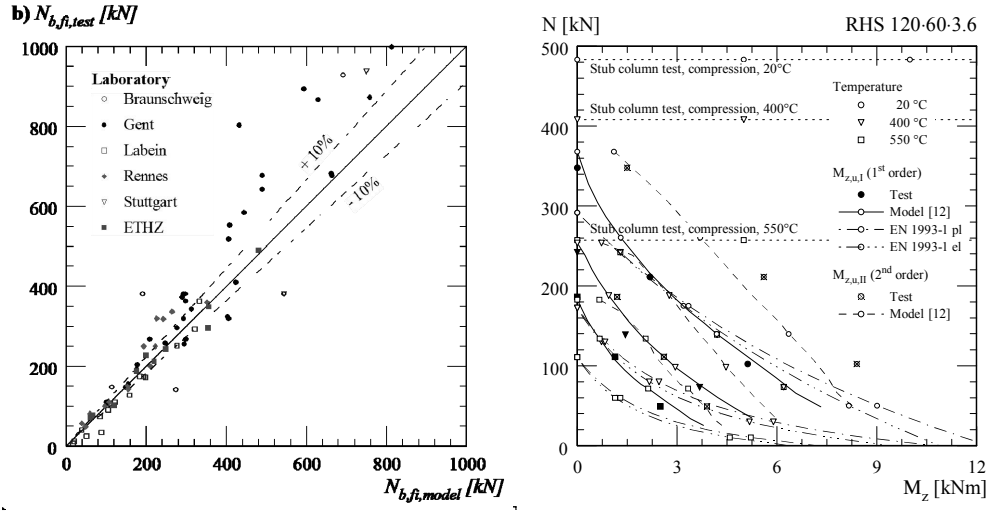

Figure 6: Comparison between slender column test results [13] and results according to the analytical model [12] (left); N-M interaction curves of the slender column tests performed at ETH and according to the analytical model [12] and the European fire design model [5] (right).

4 COMPARISON OF SLENDER COLUMN TESTS AND ANALYTICAL MODELS

Simple European fire design models [5] for steel beam-columns adapt the ambient temperature design M-N interaction formulae considering a so-called European buckling curve for the fire design situation and temperature-dependent reduction factors for the Young's modulus and yield strength at 2% strain. A novel simplified analytical model for calculating the buckling strength of steel columns in fire is proposed in [12]. The model checks equilibrium for the external loads of second order acting on the deflected column and the column internal resistance forces. Using a strain-based formulation, the model facilitates to explicitly consider nonlinear material behavior, geometric imperfections and residual stresses.

Figure 6 (left) compares column strengths in fire according to the simplified analytical model [12] with results of independent full scale furnace tests [13] and the RHS slender column tests of ETH Zürich presented in the previous section. The model [12] considers the geometry, steel temperature at failure and the material properties of the test specimens if reported [13]. The comparison shows a generally good agreement between analytical prediction and tests results. However, partially missing data about the test specimens (e.g. stress-strain relationship at failure temperature and test conditions), replaced by nominal values leads to a rather large scatter. A better congruence is found for tests performed at ETH.

Figure 6 (right) shows the M-N interaction curves of the RHS 120·60·3.6 profile. The slender column furnace test results (dots), the stub column furnace test results (being an upper limit for the strengths in axial compression), the M-N interaction curves according to the European design models (dash-dotted lines) and the simplified analytical model according to [12] (continuous and dashed lines) are given. Using European buckling curves with actual geometry values and material properties lead to conservative results for the buckling strengths both at ambient and elevated temperatures. The very small geometric imperfections seem to be a reason for the higher strengths reached experimentally, in particular for the ambient temperature test. The simplified analytical model considers the actual imperfection values as well as the nonlinear material behavior resulting in accurate results for the M-N interaction compared to the test results for the interaction curves considering bending moments $M_{z,u,I}$. Slightly different deflections at ultimate axial load between the simplified analytical prediction and the test measures lead to somewhat less accurate results of the analytical model for calculating the bending moment $M_{z,u,II}$.

5 CONCLUSIONS

The structural stability behavior of steel columns in fire has been analytically and experimentally analyzed and the cross-sectional capacity and overall flexural buckling behavior of square and rectangular hollow sections at elevated temperatures have been determined. The experimental program comprised material tests at elevated temperatures, stub column furnace tests in pure axial compression and slender column buckling furnace tests in concentric and eccentric compression at different temperatures and strain rates. Results, including full axial load-end shortening curves have been presented. The strain rate markedly influenced the stress-strain behavior and the local and global buckling behavior. The influence of the nonlinear stress-strain relationship of steel at elevated temperatures on cross-sectional capacity, critical buckling load and overall buckling strength need to be considered for more slenderness ratios at elevated than at ambient temperatures. The stub column results show that the use of the actual area and the temperature-dependent stress at 2% strain leads to unconservative results for the cross-sectional capacity in pure compression. Further experimental and numerical studies on the cross-sectional capacity and the overall flexural buckling strengths of square and rectangular hollow sections subjected to concentric and eccentric compression will be presented on the conference.

ACKNOWLEDGEMENTS

The authors gratefully acknowledge the Swiss National Science Foundation for funding the project No. 200021-117906.

REFERENCES

[1] Twilt, L., “Stress-strain relationships of structural steel at elevated temperatures: Analysis of various options & European proposal”, TNO-report BI-91-015, ECSC project SA 112 – Part F, TNO, Delft, 1991

[2] Knobloch, M., Fontana, M. and Frangi, A., “On the interaction of global and local buckling of square hollow sections in fire”, K. Rasmussen and T. Wilkinson (ed.), Proceedings of the Fifth International Conference on Coupled Instabilities in Metal Structures CIMS2008, Sydney, Australia, 23-25 June 2008, pp. 587-594.

[3] Talamona, D., Franssen, J.M., Schleich, J.B. and Kruppa, J., “Stability of steel columns in case of fire: Numerical modeling“, Journal of Structural Engineering, 123(6), 713-720, 1997

[4] Franssen, J.M., Talamona, D., Kruppa, J. and Cajot, L.G., “Stability of steel columns in fire: Experimental Evaluation”, Journal of Structural Engineering, 124(2), 158-163, 1998

[5] EN1993-1-2, “Design of Steel Structures, Part 1-2: General Rules, Structural Fire Design”, Brussels, 2005.

[6] Toh, W.S., Tan, K.H., Fung, T.C., „Compressive resistance of steel columns in fire: Rankine approach“, Journal of Structural Engineering, 126(3), 398-405, 2000

[7] Shanley, F.R., “Inelastic column theory”, Journal Aeron, 14, 1947

[8] Engesser, F., „Knickfragen“, Schweiz. Bauzeitung, 25, 1895

[9] Kármán v., T., „Untersuchungen über die Knickfestigkeit“, Forschungshefte, VDI, H.81, 1910

[10] Hochholdinger, B., Grass, H., Lipp, A., Wahlen, A. and Hora, P., “Determination of flow curves by stack compression tests and inverse analysis for the simulation of press hardening”, Numisheet - 7th International Conference and Workshop on Numerical Simulation of 3D Sheet Metal Forming Process, Interlaken, Switzerland, 2008

[11] Pauli, J., Knobloch, M. and Fontana, M., “Stub column tests on square and rectangular hollow steel sections at elevated temperatures”, Proceedings of the Fourth International Conference on Structural Engineering, Mechanics and Computation, Cape Town, South Africa, 2010

[12] Somaini, D., Knobloch, M. and Fontana, M., “Simplified analytical model for centrically and eccentrically loaded steel columns in fire”, Proceedings of the Fourth International Conference on Structural Engineering, Mechanics and Computation, Cape Town, South Africa, 2010

[13] Schleich J.B., Cajot, L.G., Pierre, M. and Warszta, F., “Buckling curves in case of fire, Final Report, Part 1”, Esch/Alzette: PROFIL ARBED